Full length article

Multiscale modeling of the anisotropic electrical conductivity of architectured and nanostructured Cu-Nb composite wires and experimental comparison

T. Gu [a, b], J.-R. Medy [c], F. Volpi [d], O. Castelnau [a], S. Forest [b], E. Hervé-Luanco [e, b], F. Lecouturier [f], H. Proudhon [b, *], P.-O. Renault [c], L. Thilly [e]

[a] PIMM, CNRS UMR 8006, Arts et Métiers ParisTech, CNAM, 151 Bd de l'Hôpital, 75013 Paris, France
[b] MINES ParisTech, PSL Research University, MAT – Centre des matériaux, CNRS UMR 7633, BP 87 91003 Evry, France
[c] Institut Pprime, UPR 3346, CNRS, University of Poitiers, ISAE-ENSMA, SP2MI, Boulevard Marie et Pierre Curie, BP 30179, 86962 Futuroscope Chasseneuil Cedex, France
[d] Univ. Grenoble Alpes, CNRS, Grenoble INP, SIMaP, F-38000 Grenoble, France
[e] Université de Versailles, Saint-Quentin en Yvelines, 45 Avenue des Etats-Unis, F-78035 Versailles Cedex, France
[f] Laboratoire National des Champs Magnétiques Intenses, EMFL, CNRS-INSA-UGA-UPS, Grenoble & Toulouse, France

A B S T R A C T

Nanostructured and architectured copper niobium composite wires are excellent candidates for the generation of intense pulsed magnetic fields (> 90T) as they combine both high electrical conductivity and high strength. Multi-scaled Cu-Nb wires can be fabricated by accumulative drawing and bundling (a severe plastic deformation technique), leading to a multiscale, architectured and nanostructured microstructure providing a unique set of properties. This work presents a comprehensive multiscale study to predict the anisotropic effective electrical conductivity based on material nanostructure and architecture. Two homogenization methods are applied: a mean-field theory and a full-field approach. The size effect associated with the microstructure refinement is taken into account in the definition of the conductivity of each component in the composites. The multiscale character of the material is then accounted for through an iterative process. Both methods show excellent agreement with each other. The results are further compared, for the first time, with experimental data obtained by the four-point probe technique, and also show excellent agreement. Finally, the qualitative and quantitative understanding provided by these models demonstrates that the microstructure of Cu-Nb wires has a significant effect on the electrical conductivity.

1. Introduction

In recent years, two types of filamentary and multilayered nano-composites composed of copper and niobium (i.e. Cu-Nb nano-composite wires and laminates) have been highlighted for their special properties [1]. These Cu-Nb nano-composites were fabricated by two different severe plastic deformation techniques: Accumulative Drawing and Bundling (i.e. ADB, see Table 1 for the abbreviations) [2,3] and Accumulated Roll Bonding [4,5], respectively. These materials are termed nano-composites both with respect to the minimum size of the different phase elements and also to the very fine grain size obtained in each phase in the transverse cross section due to the severe plastic deformation process.

An example of Cu-Nb nano-composite wire microstructures are shown in Fig. 1. These are referred to as "Filamentary" structure in Refs. [6,7]: a multiscale Cu matrix embedding parallel Nb nano-filaments. These nano-composite conductors are excellent candidates for generation of intense pulsed magnetic fields (> 90T), which are becoming essential experimental and industrial tools [8–11]. To generate them, the conductors for the winding coils must combine both high mechanical strength and high electrical conductivity. Using this type of microstructure, a conductor presenting an ultimate tensile strength as large as 1.9 GPa at 77 K has been obtained together with an electrical conductivity of

* Corresponding author.
E-mail address: henry.proudhon@mines-paristech.fr (H. Proudhon).

http://dx.doi.org/10.1016/j.actamat.2017.08.066

Table 1
The abbreviations used in this work.

ADB	Accumulative Drawing and Bundling
GSC	Generalized Self-Consistent
FEM	Finite Element Method
PH	Periodic Homogenization
HEM	Homogeneous Equivalent Medium
RVE	Representative Volume Element

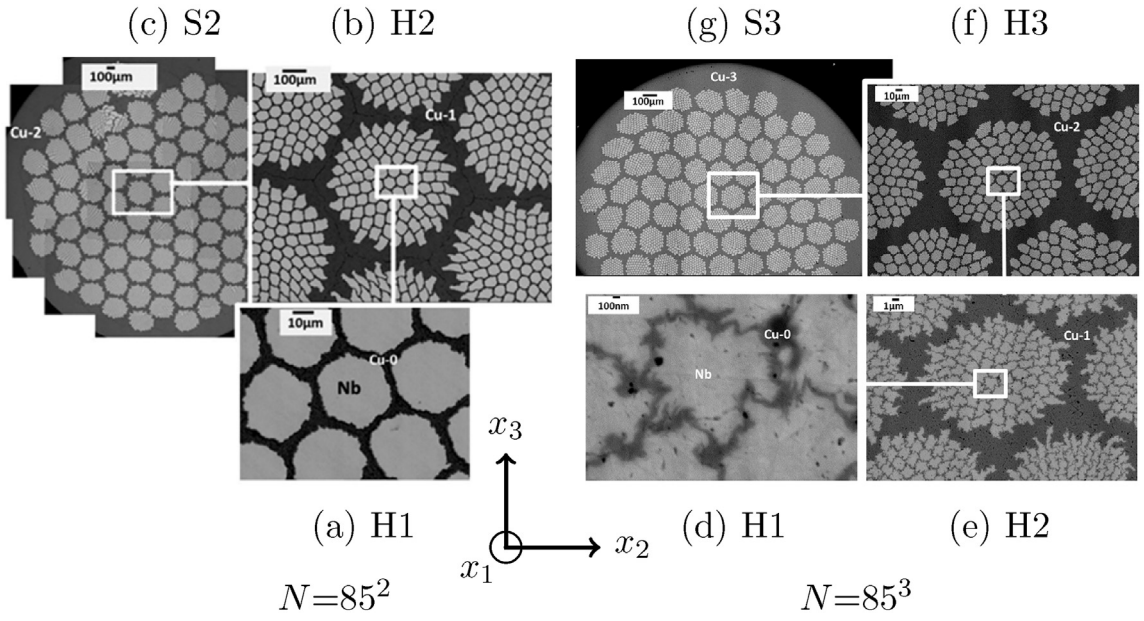

Fig. 1. Successive cross-section views of the Cu/Nb nano-composite wires containing (a–c) 85^2 and (d–g) 85^3 elementary Cu/Nb long fibers (so-called $N = 85^2$ and $N = 85^3$ type of conductor). The diameters of the specimen of (c) and (g) are 4.50 mm and 2.10 mm respectively. The diameter of specimen (c) for $N = 85^2$ and (g) 85^3 are reduced to a series of thinner ones ranging [0.25,2.10] mm and [0.55,2.10] mm respectively by supplementary cold drawing. See Section 2.2 for scale conventions and their notations.

$1.72\ \mu\Omega^{-1}\text{cm}^{-1}$ [6,12].

To predict the behavior of such a composite, the main challenge is the understanding of the complex interaction between the different material phases and the architecture, in particular when the Cu-Nb composite is fabricated by severe plastic deformations where the elementary physical deformation mechanisms are modified by grain sizes. In this field, combining material characterization and multiscale modeling is mandatory. The previous studies on the Cu-Nb nano-composite wires and laminates dealt with the mechanical behaviors [4,5,7,12–20]. In the present work, multiscale modeling will be used to study the anisotropic electrical conductivity of these architectured and nanostructured Cu-Nb composite wires, then the theoretical results will be compared with experimental data using the four-points probe technique.

Multiscale modeling of the electrical conductivity of composite materials is a complex topic, particularly if microstructural features lead to a size effect in electronic conduction and create an anisotropy [21–23]. The conductivity of both Cu and Nb single crystals are isotropic due to their cubic crystal structure (Face-Centered Cubic, i.e. FCC, for Cu and Body-Centered Cubic, i.e. BCC, for Nb) [24,25]. Furthermore, the grain boundaries and the microstructure refinement of each individual Cu/Nb component lead to size effect, as additional scattering of conduction electrons occurs at internal interfaces (i.e. Cu/Cu, Nb/Nb and Cu/Nb interfaces). For instance Lu et al. measured the conductivity for equiaxed polycrystalline Cu with different grain sizes [26]: (i) as small as 30 nm; (ii) varying from ~100 nm to 1 μm; (iii) lager than 100 μm. It was found that (ii) and (iii) exhibit similar conductivity (percentage difference[1]<5%), and that their conductivity is ~10 to 100 times (depending on the temperature) as large as the one of (i) due to the effect of grain boundaries. In analogy to scattering at the surface in an infinite long fiber with a small diameter, the size effect was experimentally confirmed and can be modeled [27–33]. Based on Dingle's model [28], Thilly [6] takes the temperature, dislocation density and size effect into account for predicting the conductivity of Cu-Nb wires along the wire direction (denoted *longitudinal* direction in this work and corresponding to the x_1-axis).

In order to predict the *anisotropic* effective conductivity of fiber-reinforced composites (such as Cu-Nb wires at different scales in Fig. 1), several homogenization models have been proposed. The homogenization models for composites can be separated into two types: mean-field analytical methods [34–37] and full-field ones [23,38]. Among the mean-field models, the Generalized Self-Consistent scheme (denoted GSC hereafter) was initially developed to study the elastic behavior of multi-coated fiber-reinforced composites [39]. Later, the GSC scheme was extended for diffusion phenomena [37,40,41], and this model has been found to be very efficient to estimate the effective electrical conductivity of Cu-Nb wires [19]. As for the full-field analysis, we have proposed a Finite Element Method (FEM) method with periodic boundary conditions (denoted PH, for Periodic Homogenization) [19]. FEM PH is adapted to the case of periodic fiber distribution, as observed experimentally (see Fig. 1), but it costs more CPU time compared with the GSC scheme.

Finally, the theoretical studies of electrical conductivity need to be validated by experimental data. To measure electrical conductivity of materials with microstructure size ranging from nanometer to millimeter, the four-point probe technique has been

[1] Percentage difference (in %): the absolute difference between two values divided by their average.

developed using separate pairs of current-carrying and voltage-sensing electrodes to avoid series resistances due to local contact and cables [42,43]. This technique is available for different sample geometries, e.g. nano-wires [33,44] and thin films [45,46]. Making use of the four-point probe technique, Thilly and Dubois have reported the conductivity of the bulk highly hardened Cu/Nb separately and Cu-Nb wires along the wire direction (i.e. longitudinal conductivity) [6,47].

Despite numerous works in literature on the electrical conductivity of composites materials, we have found that the following two points are still missing: 1. no hierarchical homogenization strategy was developed to predict the *anisotropic* electrical conductivity of recent Cu-Nb wires, taking into account the complex architectures (i.e. the multi-scaled fiber-reinforced microstructure) and the size effect; 2. to date, no experiments were carried out to determine the *anisotropic* electrical properties of Cu-Nb wires, particularly the properties in the *transverse* direction (i.e. perpendicular to the wire direction x_1), in order to validate the theoretical predictions.

Therefore, the objectives of this paper are twofold: 1. provide a multiscale homogenization procedure to predict the anisotropic effective electrical conductivity of Cu-Nb wires; 2. validate homogenization models by comparing with experimental data in both longitudinal and transverse directions. It is worth noting that, for the application of Cu-Nb wires, i.e. winding coils, only the *longitudinal* electrical properties are needed. On the other hand, many different physical problems in steady state, such as electrical conductivity, thermal conduction, diffusion and magnetism, share the same constitutive relation between the potential field and its current [48,49]. In other words, for fiber-reinforced materials (e.g. Cu-Nb wires), the above-mentioned phenomena are equivalent meaning that their *anisotropic* effective properties can be predicted also by the proposed hierarchical homogenization strategy.

The outline of the article is as follows. The architecture and nano-structure of Cu-Nb composite wires are described in Section 2. Experimental methods for the anisotropic electrical property characterization are briefly presented in Section 3. In order to reproduce the effective behavior of this material, two multiscale methods (i.e. GSC and PH) and an iterative scale transition strategy are presented in Section 4. In Section 5, anisotropic model responses are compared with experimental data. Finally, the relation between the effective material behavior and its microstructure is discussed.

2. Material description

2.1. Fabrication process

Cu-Nb nano-composite wires were fabricated via a severe plastic deformation process, based on ADB (i.e. series of hot extrusion, cold drawing and bundling stages) [2,3]: a Nb wire is inserted into a Cu tube; the structure is extruded and drawn, then cut into 85 smaller pieces with hexagonal cross section; these pieces are then bundled and inserted into a new Cu tube; the new composite structure is again extruded and drawn. And so on. In the present work, ADB is repeated two or three times, leading to copper based architectured and nanostructured composite wires which are composed of 85^2 (Fig. 1(a–c)) and 85^3 (Fig. 1(d–g)) Nb nanofibers. They are the so-called $N = 85^2$ and $N = 85^3$ type of Cu-Nb "Filamentary" wires respectively [50]. The used Cu is Oxygen-Free High Conductivity (OFHC).

It is noted that, unlike Cu, Nb fibers are introduced only at the very first fabrication stage. Therefore, Nb fibers (Fig. 1(a) and (d)) are all deformed together during the iterative ADB process, and they exhibit the same microstructure and similar characteristic sizes. In contrast, the Cu-0 regions (Fig. 1(a)) are introduced at the beginning of the process, while the Cu-1 and Cu-2 (Fig. 1(b–c)) are introduced successively during the two steps of ADB for $N = 85^2$. It is similar for the Cu components in $N = 85^3$ (Fig. 1(d–g)). Thus different microstructure are expected for different Cu-i regions (i = 0,1,2 and 3).

Table 2
Volume fraction $f^{(i)}$ and theoretical dimensions $\delta^{(i)}$ of each component i in the case of conductor diameter $d = 0.25$, 2.10 mm for $N = 85^2$ and $d = 0.55$, 2.10 mm for $N = 85^3$, with the corresponding conductivity $\sigma^{(i)}$ ($\mu\Omega^{-1}\text{cm}^{-1}$) at 293 K.

Phase i	$f^{(i)}$	$\delta^{(i)}$	$\sigma^{(i)}$	$\delta^{(i)}$	$\sigma^{(i)}$
$N = 85^2$		$d = 0.25$ mm		$d = 2.10$ mm	
Nb	44.7%	1.67 μm	0.060	13.74 μm	0.060
Cu-0	15.2%	0.27 μm	0.508	2.19 μm	0.561
Cu-1	17.5%	2.67 μm	0.562	21.97 μm	0.568
Cu-2	22.6%	15.14 μm	0.567	124.48 μm	0.568
$N = 85^3$		$d = 0.55$ mm		$d = 2.10$ mm	
Nb	34.5%	323.8 nm	0.060	1.22 μm	0.060
Cu-0	11.8%	50.9 nm	0.327	192.2 nm	0.485
Cu-1	13.6%	511.8 nm	0.537	1.93 μm	0.560
Cu-2	17.5%	5.82 μm	0.565	21.97 μm	0.568
Cu-3	22.6%	32.99 μm	0.568	124.48 μm	0.568
bulk Cu		∞	0.568	∞	0.568
bulk Nb		∞	0.060	∞	0.060

In this work, the above-mentioned two types of Cu-Nb conductor are studied with different diameters[2]: $d \in [0.25, 2.10]$ mm for $N = 85^2$ and $d \in [0.55, 2.10]$ mm for 85^3. The volume fraction $f^{(i)}$ of each type of conductor is not changed by hot-extrusion and cold-drawing and they can be determined by the initial dimensions of Nb cylinder and Cu jacket. The theoretical value of channel width, $\delta^{(i)}$, can be estimated by supposing that all the perfect and concentric components (i.e. Nb cylinder and Cu tube) are deformed in a homothetic way during material processing [3]. Table 2 indicates the volume fraction $f^{(i)}$ and theoretical channel width $\delta^{(i)}$ in the two extreme diameter cases (i.e. $d = 0.25$ and 2.10 mm for $N = 85^2$; $d = 0.55$ and 2.10 mm for 85^3).

2.2. Scale conventions

For $N = 85^2$ and 85^3 types of Cu-Nb nano-composite wires, Nb fibers are separated by the finest Cu-0 copper channels (see Fig. 1(a) and (d)); groups of 85 Nb/Cu-0 elementary long fibers are separated by Cu-1 copper channels (Fig. 1(b) and (e)). As illustrated in Fig. 1(f), for $N = 85^3$, groups of 85^2 elementary patterns are separated by Cu-2 channels. Finally, $N = 85^2$ patterns and $N = 85^3$ patterns are embedded respectively in an external Cu-2/Cu-3 copper jacket (Fig. 1(c) and (g)).

For multiscale modeling of the effective electrical conductivity of these Cu-Nb wires, the following scale conventions will be used: (1) Homogenization of the assembly of 85^1 elementary Nb/Cu-0 long fibers is labeled as H1 (Homogenization 1); (2) Iterative homogenization of the effective Cu-Nb composite zone of H(n-1) embedded in the Cu-(n-1) matrix (n = 2 for $N = 85^2$ and n = 2,3 for $N = 85^3$), is labeled as Hn (Homogenization n, n = 2 and 3). In other words, Hn provides the effective behavior of an assembly of 85^n elementary patterns. The effective electrical conductivity tensors, denoted $(\widetilde{\underline{\sigma}})_{Hi}$ (i = 1,2,3) at scales Hi of assembly of 85^i ($i = 1,2,3$) elementary patterns, will be obtained by homogenization

[2] Following [7, 50], all dimensions are given in the x2-x3 cross-section, i.e. perpendicular to the wire axis x1, see Fig. 1 for the coordinate system.

models.

Finally, the scales S2 and S3 (i.e. macro-scale) for $N = 85^2$ and 85^3 respectively are defined as a single cylinder-shape structure with two layers: effective Cu-Nb composite zones containing 85^2/85^3 elementary patterns (i.e. Cu-Nb H2/H3 zone) surrounded by the external Cu-2/Cu-3 jacket. The structural problem (label "S" stands for Structural) will be solved by FEM to compute the apparent material electrical conductance. Then the conductance will be compared with experimental data.

2.3. Conductivity of individual components

The Cu-Nb wires are made of FCC Cu and BCC Nb polycrystalline components, i.e. Nb, Cu-0, Cu-1, Cu-2 and Cu-3. Electrical conductivity in a single BCC/FCC grain is isotropic due to its cubic crystal structure [24,25]. In addition, the Cu/Nb grains exhibit highly elongated shapes due to the material processing, leading to an anisotropic grain boundary density (grain boundary density along $x_{2,3}$ is higher than the one along x_1) [50]. However, the influence of grain boundary is rather small on the conductivity of the polycrystalline Cu [26], as the Cu grain width varies from ~100 nm to 1 μm and the grain length is larger than 100 μm in actual Cu-Nb wires [50]. Therefore, the effective conductivity of individual polycrystalline Cu component in Cu-Nb wires is considered to be isotropic. For the sake of simplicity, conductivity of polycrystalline Nb is also supposed to be isotropic disregarding the grain boundary effect. It will be shown that these approximations are sufficient to predict the anisotropic electrical conductivity for Cu-Nb wires based on experimental comparisons.

To predict the electrical conductivity of the individual component in the Cu-Nb wires, temperature, dislocation density and size effect (i.e. channel width δ between two Cu/Nb interfaces) need to be taken into account [6]. The conductivity of bulk specimen of highly hardened Cu and Nb has also been measured [6]: $\sigma_{\text{bulk}} = 0.568\ \mu\Omega^{-1}\text{cm}^{-1}$ and $0.060\ \mu\Omega^{-1}\text{cm}^{-1}$ for Cu and Nb respectively at 293 K (reported in Table 2). It is worth noting that the highly hardened bulk specimen exhibit extremely high dislocation density, probably almost saturating. This approximately corresponds to the dislocation density case of the Cu/Nb components in Cu-Nb wires, in the considered range of conductor diameters $d \in (0.2, 2.5)$ mm.

Regarding the effect of the channel width δ, it is useful to relate the conductivity in a given phase with ℓ the mean the free path of electrons [6,51]:

$$\ell_{Cu}(T) = 66\,\sigma_{bulk-Cu}(T) \tag{1a}$$

$$\ell_{Nb}(T) = 87\,\sigma_{bulk-Nb}(T) \tag{1b}$$

(with σ_{bulk} in $\mu\Omega^{-1}\text{cm}^{-1}$ and ℓ in nm). The mean free path of electrons ℓ is defined as the average distance travelled by a moving electron between successive collisions. Dingle's model [28] has been initially developed to predict the conductivity of an infinite long fiber with a small diameter δ. In the present case, the conductivity of the long fiber is strongly affected by the transverse dimension due to electron scattering at surfaces/interfaces. The model was later extended in terms of the ratio δ/ℓ [6]:

$$\frac{\sigma}{\sigma_{bulk}} = \frac{\delta}{\ell} - \frac{3}{8}\left(\frac{\delta}{\ell}\right)^2\left[\ln\left(\frac{\ell}{\delta}\right) + 1.059\right] \quad for \quad \delta < 0.467\ell \tag{2a}$$

$$\frac{\sigma}{\sigma_{bulk}} = \left(1 + \frac{\ell}{\delta}\right)^{-1} \; for\; \delta \in [0.467\ell, 3, \ell[\,, \tag{2b}$$

$$\frac{\sigma}{\sigma_{bulk}} = 1 - \frac{3}{4}\frac{\ell}{\delta} \quad for \quad \delta > 3\ell\,. \tag{2c}$$

The conductivity $\sigma^{(i)}$ of individual component i is determined by the choice of one of the three above equations which are expressed in terms of the theoretical channel width $\delta^{(i)}$ of this component. Table 2 reports the conductivity $\sigma^{(i)}$ calculated by Equations (1) and (2) of each individual component with the corresponding channel width $\delta^{(i)}$ at 293 K. It is worth noting that the characteristic channel width $\delta^{(i)}$ plays the same role on the additional scattering of the electrons conducted along both the *longitudinal* and *transverse* directions. Therefore, taking into account the size effect, $\sigma^{(i)}$ can still be supposed to be *isotropic*.

3. Experimental methods

Macroscopic *longitudinal* conductivities of the considered Cu-Nb wires were determined previously [6,50] and are reported here for completeness. A series of samples are used with a length of 40 cm and a variable diameter d (see Section 2.1). The conductivities of these samples are measured by the four-point probe technique at 293 K: the two outer current-carrying probes are placed at both ends of the wire, then the two inner voltage-sensing ones are placed between them; the distances between the outer probes and inner probes are 39 cm and $L = 36.8$ cm respectively. A current $I = 0.1$ A is injected by the outer pair and the potential difference ΔU is measured by the inner pair leading to the following experimental longitudinal conductivity σ_{L}:

$$\sigma_{\text{L}} = \frac{I}{\Delta U}\cdot\frac{L}{S} \tag{3}$$

where the ratio $I/\Delta U$, L and S are the electrical conductance, the distance between the voltage-sensing probes and the sectional area respectively. The reported value is the average measurement with an uncertainty on the order of 5% [6,50].

Due to ADB processing, the architecture of Cu-Nb wires is quasi-axisymmetric with respect to x_1. As a result, the effective material behavior is expected to be *transverse isotropic* [19,20]. For the conductivity along the *transverse* direction x_2 or x_3, a more delicate measurement is needed due to the small sample size, compared with the measurement of longitudinal conductivity [50]. The specific structure which is composed of Cu-Nb composite zone and a Cu jacket (e.g. Fig. 1(c)) must be considered.

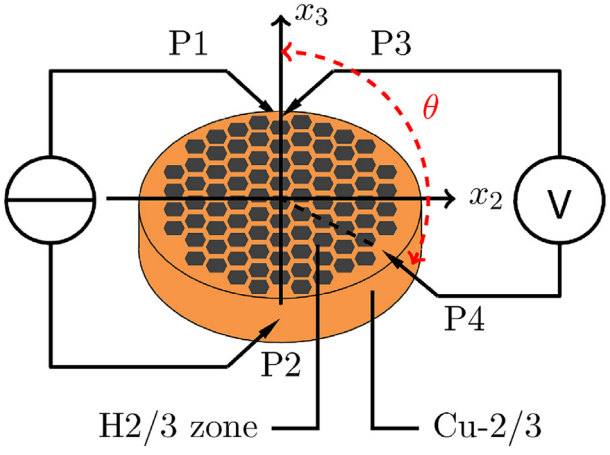

Fig. 2. Schematic of the Cu-Nb sample geometry used for the measurement of transverse electrical conductance.

The measurement of *transverse electrical conductance* is also performed with the four-point probe for both $N = 85^2$ and 85^3 Cu-Nb wires with a diameter of $d = 2.10$ mm at 293 K [50]. The cylinder-shape S2/S3 samples have been cut and mechanically polished on two parallel sides perpendicular to x_1 down to 218±5 μm and 190±5 μm for $N = 85^2$ and 85^3 respectively (Fig. 2). The two fixed current-carrying probes P1 and P2 are placed along the diameter x_3 outside the Cu-2/Cu-3 jacket, on the side walls of the samples (i.e. $x_2 = 0$, $x_3 = \pm 1.05$ mm for P1 and P2), as illustrated in Fig. 2. The two voltage-probes P3 and P4 are placed on the upper surface. P3 is fixed in the middle of Cu-2/Cu-3 ring along the diameter x_3. In order to investigate the electrical conductance of the whole sample, the mobile probe P4 is positioned on the upper surface along two different paths: (i) along a diameter (i.e. along x_3 axis with $x_3 \in [-1.05, 1.05]$ mm); (ii) along the middle line of Cu-2/Cu-3 ring (i.e. position described by an angle θ in a cylindrical coordinate system with $\theta \in [0\ ^\circ, 180\ ^\circ]$), as shown in Fig. 2.

The injected current I at P1 and P2 was scanned from −0.1 A to 0.1 A with a Keithley 6221 power source. Then the electric potential difference $\Delta U = U_{P3} - U_{P4}$ was measured between the fixed P3 and the mobile P4 with a nanovoltmeter Agilent 34420. The uncertainties of the measured apparent conductance is estimated as small as $\pm 0.1\ \mathrm{m}\Omega^{-1}$ (fit uncertainty of the $I/\Delta U$ data set). On the other hand, the position uncertainties of mobile P4 are estimated as ±0.1 mm and ±9 ° for P4 position along the x_3 diameter and along the Cu-2/Cu-3 ring respectively due to the small sample sizes. The experimental data will be shown and compared with model predictions, in the longitudinal (Section 5.1) and transverse directions (Section 5.2).

4. Hierarchical homogenization strategy

In this section, the effective electrical conductivity of Cu-Nb wires will be predicted taking into account the specific multi-scaled fiber-reinforced material architecture. At the effective scale H1, (Fig. 1(a) and (d)), the elementary patterns appear with two layers: Nb cylinder and Cu-0 tube. In order to homogenize the assembly of these 85^1 Nb/Cu-0 fibers, a mean-field homogenization method and a full-field FEM approach will be presented in Section 4.1 and Section 4.2 respectively. As the specimens exhibit many characteristic scales (i.e. H1, H2, H3), a hierarchical homogenization strategy will be proposed in Section 4.3.

4.1. Mean-field generalized self-consistent scheme

The GSC scheme [19,37] is developed in the following way: (i) (n+1)-layered cylindrical problem and (ii) n-layered problem embedded in the HEM where the effective electrical conductivity $\widetilde{\underline{\sigma}}$ is determined by the self-consistent scheme [40,52], as illustrated in Fig. 3(a). When applied to estimate the effective electrical conductivity of H1, this scheme assumes that the elementary Nb/Cu-0 fibers are distributed randomly.

Following [39], component 1 constitutes the central core and component i lies within the shell limited by the two concentric cylinders with the radii R_{i-1} and R_i ($R_0 = 0$).

Each component is assumed to be homogeneous and to exhibit a transverse isotropic behavior with the axis of symmetry along the wire direction x_1. We denote the longitudinal and transverse electrical conductivity by $\sigma_{\mathrm{L}}^{(i)}$ and $\sigma_{\mathrm{T}}^{(i)}$ respectively in the component i. The transverse isotropic conductivity is expressed as a second order tensor: $\underset{\sim}{\boldsymbol{\sigma}}^{(i)} = \sigma_{\mathrm{T}}^{(i)}\,(\underline{e}_2 \otimes \underline{e}_2 + \underline{e}_3 \otimes \underline{e}_3) + \sigma_{\mathrm{L}}^{(i)}\ \underline{e}_1 \otimes \underline{e}_1$ where $\otimes$ denotes the tensor product. Each component i obeys Ohm's law:

$$\underline{j}^{(i)} = -\underset{\sim}{\boldsymbol{\sigma}}^{(i)} \cdot \nabla\, U^{(i)} = \underset{\sim}{\boldsymbol{\sigma}}^{(i)}\, \underline{E}^{(i)} \tag{4}$$

where U, $\underline{j}$ and $\underline{E}$ denote the electric potential (μV), current density ($A\ \mathrm{mm}^{-2}$) and the electric field ($\mu\mathrm{V\ mm}^{-1}$) respectively. Furthermore, in each individual Cu/Nb component i, the conductivity is isotropic leading to $\sigma_{\mathrm{L}}^{(i)} = \sigma_{\mathrm{T}}^{(i)}$, as mentioned in Section 2.3. On the other hand, the assembly of long fibers at H1 exhibit a transverse isotropic effective conductivity [19].

The detailed GSC derivation of the effective conductivity $\widetilde{\underline{\sigma}}$ of the

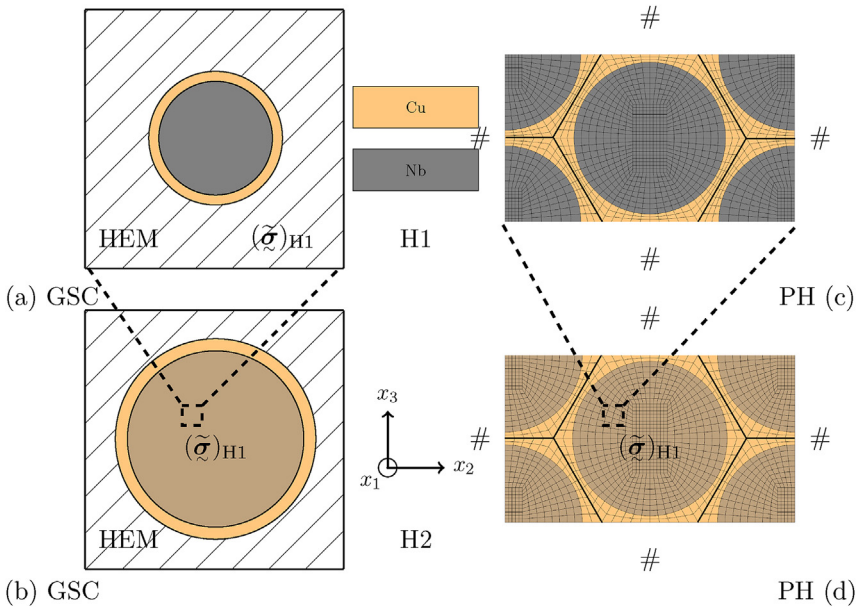

Fig. 3. Multiscale modeling of the effective conductivity from scale H1 (a and c) to scale H2 (b and d). (a–b): The iterative process by the GSC scheme; (c–d): PH with the meshes by FEM. Periodic boundary conditions in PH, denoted #, are considered. Orange stands for Cu, gray for Nb and brown for Cu-Nb composite. (For interpretation of the references to colour in this figure legend, the reader is referred to the web version of this article.)

n-layered elementary fibers can be found in Refs. [19,37]. Here, due to the morphology of Cu-Nb filamentary wires, the two-layered elementary fibers (i.e. $n = 2$) will be considered. In this particular case, the effective *transverse* conductivity reads [37]:

$$\widetilde{\sigma}_{\mathrm{T}} = \frac{\sigma_{\mathrm{T}}^{(2)}\left[R_2^2\left(\sigma_{\mathrm{T}}^{(2)} + \sigma_{\mathrm{T}}^{(1)}\right) - R_1^2\left(\sigma_{\mathrm{T}}^{(2)} - \sigma_{\mathrm{T}}^{(1)}\right)\right]}{R_2^2\left(\sigma_{\mathrm{T}}^{(2)} + \sigma_{\mathrm{T}}^{(1)}\right) + R_1^2\left(\sigma_{\mathrm{T}}^{(2)} - \sigma_{\mathrm{T}}^{(1)}\right)\Big]} \tag{5}$$

where component 1 and 2 indicate here Nb and Cu-0 respectively and R_1 and R_2 denote the radius of Nb cylinder and the external radius of Cu-0 tube respectively. In the case of effective *longitudinal* conductivity $\widetilde{\sigma}_{\mathrm{L}}$, GSC scheme leads to the following expression:

$$\widetilde{\sigma}_{\mathrm{L}} = \sum f^{(i)}\, \sigma_L^{(i)} \tag{6}$$

where $f^{(i)}$ denotes the volume fraction of component i. It should be noted that Eq. (6) is nothing else but the rule of mixture for conductivity. It is the exact solution of the longitudinal conductivity for all the microstructures formed by parallel long fibers despite their distributions [22]. Thus, this solution does not depend on the homogenization method used.

4.2. Full-field periodic model

The mean-field GSC scheme, presented in the previous section, assumes a random distribution of coated long fibers. In order to take into account the quasi-periodic fiber distribution observed experimentally (Fig. 1) due to the material processing and to investigate the effect of this particular distribution, a periodic problem needs to be solved. As mentioned in Refs. [19,20,53,54], a unit cell subjected to periodic boundary conditions was considered and this problem was solved using FEM PH. The periodicity of unit cell and boundary conditions allow us to determine the effective conductivity $\underset{\sim}{\widetilde{\boldsymbol{\sigma}}}$ in a periodic and infinite HEM.

The section views of the unit cell of scale H1 and scale H2, with their FE 3D meshes (c3d20 elements[3]), are respectively indicated in Fig. 3(c) and (d). The Z-set software[4] is used to perform the FE simulations of PH model. The unit cell contains all the information about the morphological RVE (Representative Volume Element) at the effective scales H1 and H2. These meshes are composed of two equivalent long fibers ($1 + 4 \times 1/4$ fibers) which are arranged in a hexagonal lattice, and they represent the (idealized) multi-scaled experimental microstructure of Cu-Nb wires. It should be noted that the real architecture of Cu-Nb wires at all scales contains only a finite number (i.e. 85) of long fibers. We have verified with the help of a larger hexagonal structure without periodic boundary conditions that the assumed infinity does not significantly affect our results. The mesh density has also been checked to ensure adapted numerical accuracy.

Using periodic boundary conditions, the electric potential U in the elementary volume V takes the following form:

$$U = \langle \nabla\, U \rangle \cdot \underline{x} \; + t \qquad \forall\, \underline{x} \in V \tag{7}$$

where $\langle \nabla\, U \rangle$ indicates the volume average of the electric field in V in Eq. (7), the fluctuation t is periodic, i.e. it takes the same values at two homologous points on opposite faces of V. Furthermore, the scalar of current density $\underline{j} \cdot \underline{n}$ takes opposite values at the two homologous points on opposite faces of V ($\underline{n}$ is the outwards normal vector to ∂V). In order to determine the two components of effective conductivity (i.e. $\widetilde{\sigma}_{\mathrm{L}}$ and $\widetilde{\sigma}_{\mathrm{T}}$), two electric fields $\underline{E}$ are subjected successively to V: $\langle \nabla\, U \rangle = E_0\, \underline{e_1}$ for the longitudinal conductivity $\widetilde{\sigma}_{\mathrm{L}}$, and $\langle \nabla\, U \rangle = E_0\, \underline{e_2}$ (or $E_0\, \underline{e_3}$) for the transverse one $\widetilde{\sigma}_{\mathrm{T}}$. Then the average current density $\langle \underline{j} \rangle$ is determined by numerical homogenization leading to the effective conductivity $\underset{\sim}{\widetilde{\boldsymbol{\sigma}}}$ of PH by using the following equation:

$$\langle \underline{j} \rangle = -\underset{\sim}{\widetilde{\boldsymbol{\sigma}}} \cdot \langle \nabla\, U \rangle \,. \tag{8}$$

4.3. Scale transition strategy

Both GSC scheme and FEM PH are applied at the effective scale H1 taking the size effect into account by the definition of $\underset{\sim}{\boldsymbol{\sigma}}^{(i)}$ of each individual Cu/Nb component (see Table 2). It is found that the effective electrical conductivity $(\underset{\sim}{\widetilde{\boldsymbol{\sigma}}})_{H1}$ obtained by the two models are in a very good agreement (percentage difference $\sim$1.0%). This result allows an accurate prediction of the effective conductivity at larger scales (i.e. scale H2/H3).

At scale H2 (Fig. 1(b)(e)), the effective long fibers consists of two layers: (1) the nano-composite Cu-Nb zones containing 85^1 parallel elementary fibers (i.e. H1 zones) and (2) the Cu-1 matrix. As illustrated in Fig. 3, an iterative process is proposed. The electrical conductivity of the inner layer at scale H2, $(\underset{\sim}{\boldsymbol{\sigma}}^{(1)})_{\mathrm{H2}}$, is given by the effective tensor $(\underset{\sim}{\widetilde{\boldsymbol{\sigma}}})_{H1}$ at H1. On the other hand, $(\underset{\sim}{\boldsymbol{\sigma}}^{(2)})_{\mathrm{H2}}$ of the second layer for H2 is associated with the conductivity of Cu-1 $(\underset{\sim}{\boldsymbol{\sigma}})_{\mathrm{Cu\text{-}1}}$. The scale transition is then performed by GSC and PH approaches, leading to the effective conductivity $(\underset{\sim}{\widetilde{\boldsymbol{\sigma}}})_{H2}$ for the assembly of 85^2 elementary long fibers. The same iterative process will be repeated up to H3 for $N = 85^3$ conductors using the same models, allowing to estimate $(\underset{\sim}{\widetilde{\boldsymbol{\sigma}}})_{H3}$.

The transverse isotropic effective conductivity $(\underset{\sim}{\widetilde{\boldsymbol{\sigma}}})_{H2}$ (for $N = 85^2$) and $(\underset{\sim}{\widetilde{\boldsymbol{\sigma}}})_{H3}$ (for $N = 85^3$) at 293 K are shown in Fig. 4(a) and Fig. 4(b) respectively. The decrease in conductivity $\underset{\sim}{\widetilde{\boldsymbol{\sigma}}}$ with the diameter d reduction is due to the channel width δ reduction associated with drawing (i.e. due to size effect, see Section 2.3). It is also found that, the magnitude of $\underset{\sim}{\widetilde{\boldsymbol{\sigma}}}$ decrease is larger for $N = 85^3$ than for $N = 85^2$ due to the higher influence of material refinement.

It is remarkable that the GSC scheme and PH provide very close results for all the diameters d of $N = 85^2/85^3$ conductors. The percentage difference between the predictions of these two models is always $\sim$1%. This good match between model responses is likely due to (i) the relatively small electrical contrast between Cu and Nb electrical conductivities and (ii) both models take into account the presence of a component playing the role of a matrix. Furthermore, similar predictions of GSC and PH demonstrate a limited influence of fiber distribution on conductivity, as these two models assume respectively a random or a periodic distribution.

5. Experimental comparison and discussion

5.1. Experimental comparison for longitudinal conductivity

In Section 3, the experimental macroscopic longitudinal conductivity by four-point probing at 293 K was recalled. Then the anisotropic effective conductivity $(\underset{\sim}{\widetilde{\boldsymbol{\sigma}}})_{\mathrm{H2}}$ of $N = 85^2$ (also for $(\underset{\sim}{\widetilde{\boldsymbol{\sigma}}})_{\mathrm{H3}}$ of

[3] c3d20: quadratic hexahedrons with 20 nodes per element.
[4] Software for finite element method – http://www.zset-software.com.

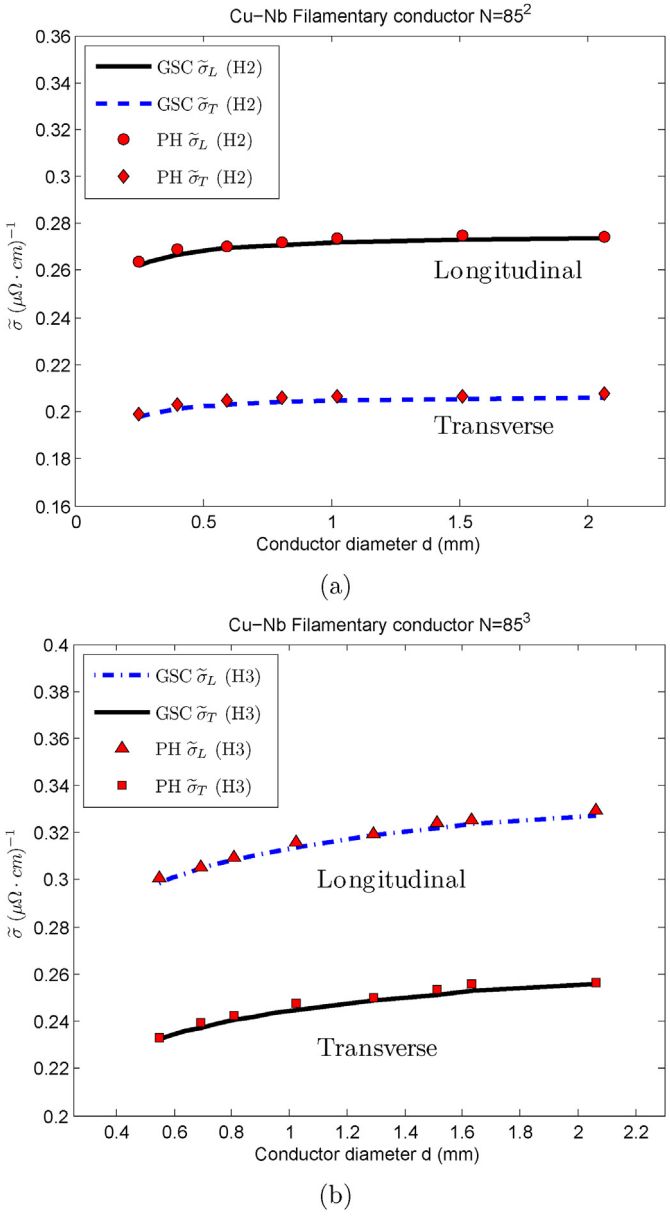

Fig. 4. Effective longitudinal and transverse conductivity of (a) H2 for $N = 85^2$ and (b) H3 for 85^3 with respect to the conductor diameter d. The curves are obtained by the Generalized Self-Consistent model (GSC) and the points by Periodic Homogenization (PH).

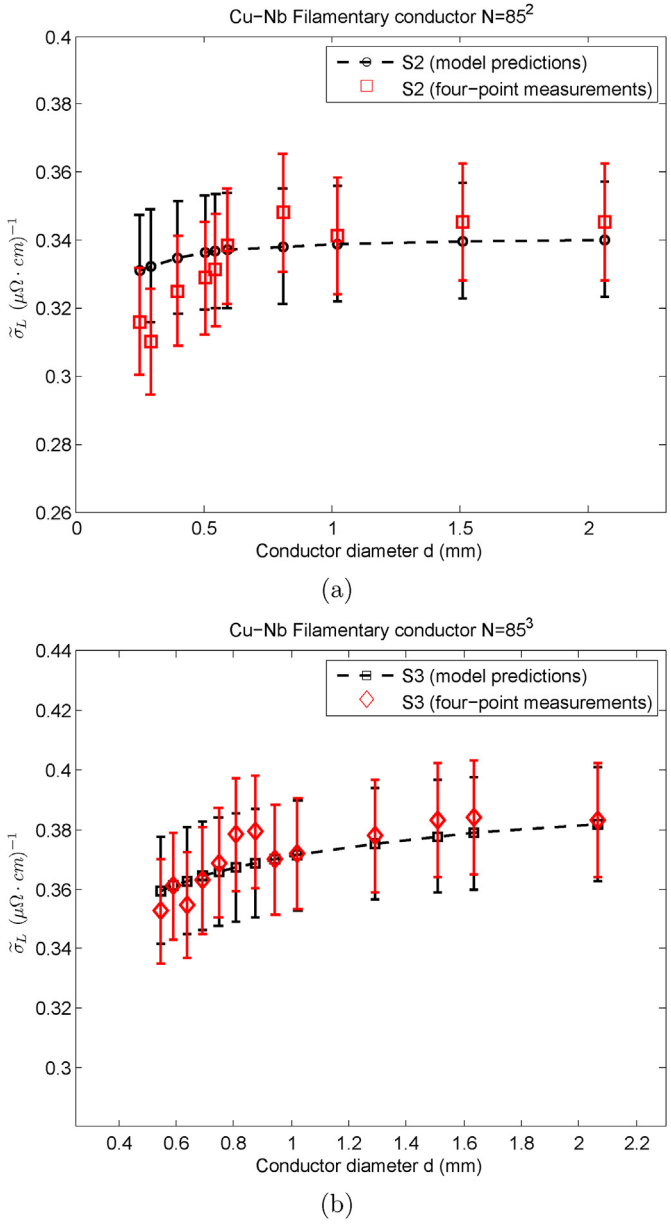

Fig. 5. Experimental data for macroscopic longitudinal conductivity compared with model predictions with various diameters d for: (a) $N = 85^2$; (b) $N = 85^3$.

$N = 85^3$) has been determined by the GSC scheme and the FEM PH method with a scale transition iterative process in Section 4.3.

Predictions of the effective macroscopic longitudinal conductivities (i.e. $(\tilde{\sigma}_L)_{S2}/(\tilde{\sigma}_L)_{S3}$ for $N = 85^2/85^3$ respectively) are compared with experimental measures shown in Fig. 5. The uncertainty of the conductivity measurement is on the order of ±5% for $(\tilde{\sigma}_L)_{S2/3}$ of Cu-Nb composite specimens [50] and for the σ_{bulk} of bulk specimens [6]. The model results depend directly on σ_{bulk} for each Cu/Nb component, the uncertainty of σ_{bulk} leads to an uncertainty of a similar magnitude on model results (i.e. ±5%) [19].

Very good agreement (percentage difference<5% in uncertainty range) is found between experiment and theory for macroscopic longitudinal conductivity of both $N = 85^2$ and 85^3 Cu-Nb wires with various conductor diameters. The longitudinal model predictions depend on the conductivity of each Cu/Nb component $(\underset{\sim}{\sigma})_{Nb/Cu\text{-}i}$ (i = 0, 1, 2, 3) and the scale transition strategy. The general good agreement between the model predictions and the experimental data supports the idea that Dingle's model (Equations (1) and (2)) correctly takes into account the size effect on the conductivity. However, some deviations can still be observed, particularly with conductor diameters $d < 0.5$ mm for $N = 85^2$ (see Fig. 5(a)). Two main reasons can explain these deviations between experiment and theory: (i) dislocation density of highly hardened bulk Cu/Nb specimen (see Section 2.3)) may not always correspond to the density in Cu-Nb wires, especially for the wires with smaller sample diameters. (ii) geometrical heterogeneity (i.e. fluctuations around the cylinders of Nb/effective cylinders of Hi zone (i = 0, 1, 2, 3) due to material processing, as observed in Fig. 1) is not considered by our models.

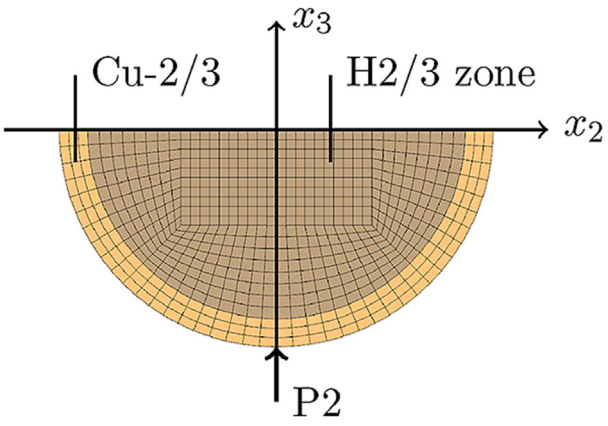

Fig. 6. Section view of the FE mesh at scale S2/S3 for $N = 85^2$ and $N = 85^3$ respectively.

5.2. Experimental comparison for transverse conductance

In Section 3, the transverse electrical conductances $I/\Delta U$ of the cylinder-shape samples have been measured by four-point probing at macro-scale (i.e. scale S2/S3 for $N = 85^2/85^3$ respectively). These data are shown in Fig. 7 with respect to the positions of the mobile point P4. Unlike the uncertainties of P4 positions, the uncertainties of the conductance measurement can be neglected. For the sake of clarity, only error-bars of the positions of P4 are plotted in Fig. 7. It should be noted that the transverse electrical *conductivity* σ_T cannot be calculated easily by an analytical approach from the measured *conductance* due to the irregular cylinder-shape sample geometry [43]. In order to compare experimental data with model predictions, structural problems (i.e. S2 and S3) need to be solved by FEM.

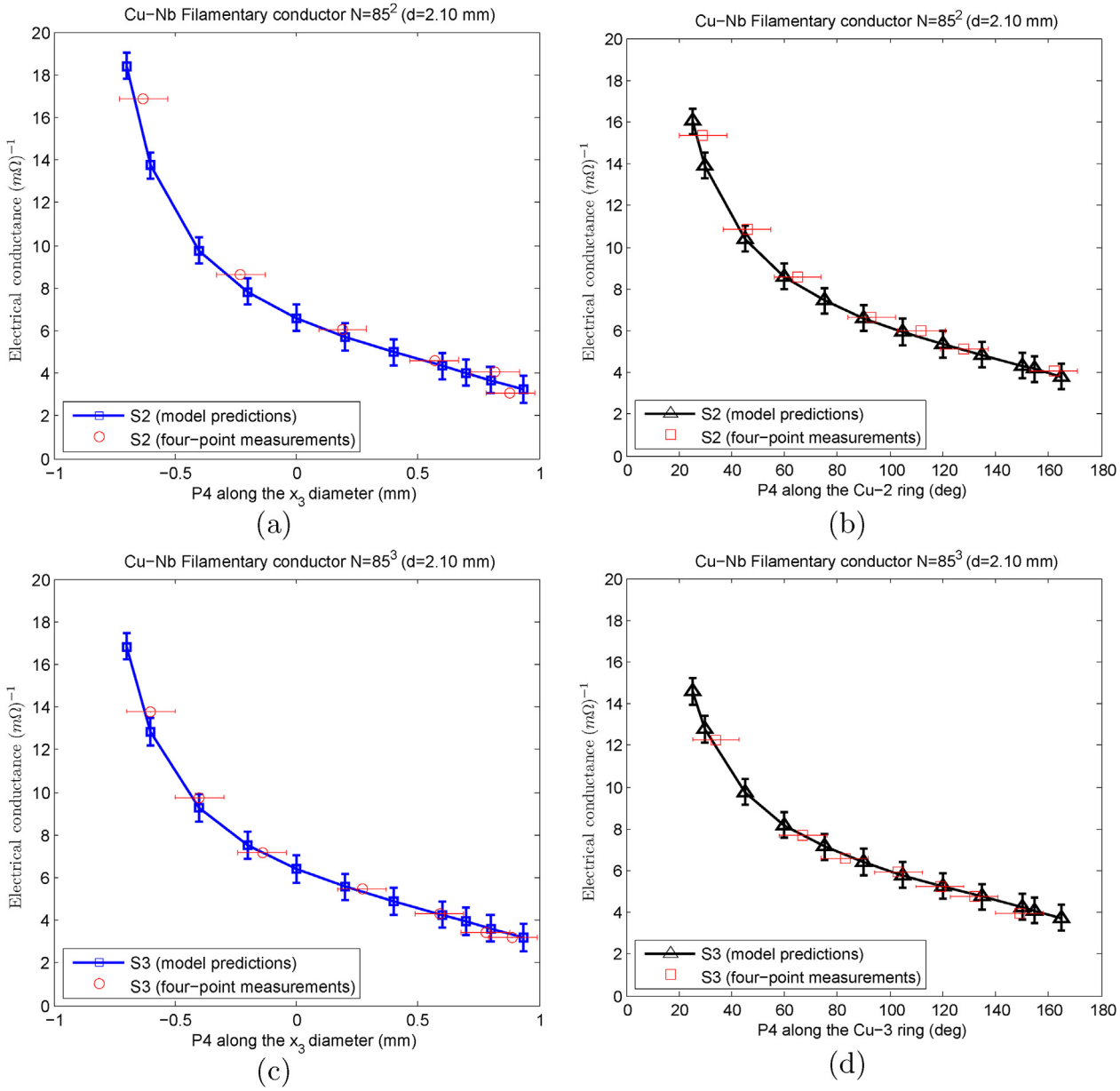

Fig. 7. Experimental transverse conductance compared with model predictions with respect to the positions of P4: (a) P4 along the x_3 diameter for $N = 85^2$; (b) P4 along the Cu-2 ring for $N = 85^2$; (c) P4 along the x_3 diameter for $N = 85^3$; (b) P4 along the Cu-3 ring for $N = 85^3$. The wire diameter d for both $N = 85^2/85^3$ is 2.10 mm.

Fig. 6 shows the 3D mesh (c3d20) using real dimensions of the S2/S3 sample to compute the apparent electrical conductance. In order to improve the computational efficiency for the S2/S3 mesh, only half of the Cu-Nb sample is simulated. Symmetric boundary conditions (i.e. electric potential $U = 0$) are imposed on the appropriate $x_3 = 0$ surface. For $N = 85^2$ Cu-Nb wires, the electrical conductivity of the inner Cu-Nb composite zone of H2 and the external Cu-2 jacket are assigned to $(\widetilde{\boldsymbol{\sigma}})_{\mathrm{H2}}$ determined in Section 4.3 and $(\widetilde{\boldsymbol{\sigma}})_{\mathrm{Cu\text{-}2}}$ (see Table 2) respectively. A similar process has been followed for $N = 85^3$. In analogy to experiments, the boundary conditions are applied to the S2/S3 mesh as follows: prescribing electric current I at P1 and P2 and computing potential U at P3 and P4 lead to the electrical conductance (as illustrated in Fig. 2). In addition, the uncertainties of the conductivity measurement for bulk specimens σ_{bulk} and of the S2/S3 sample thickness are considered, obtaining an uncertainty of conductance on the order of $\pm 0.6\ \mathrm{m}\Omega^{-1}$.

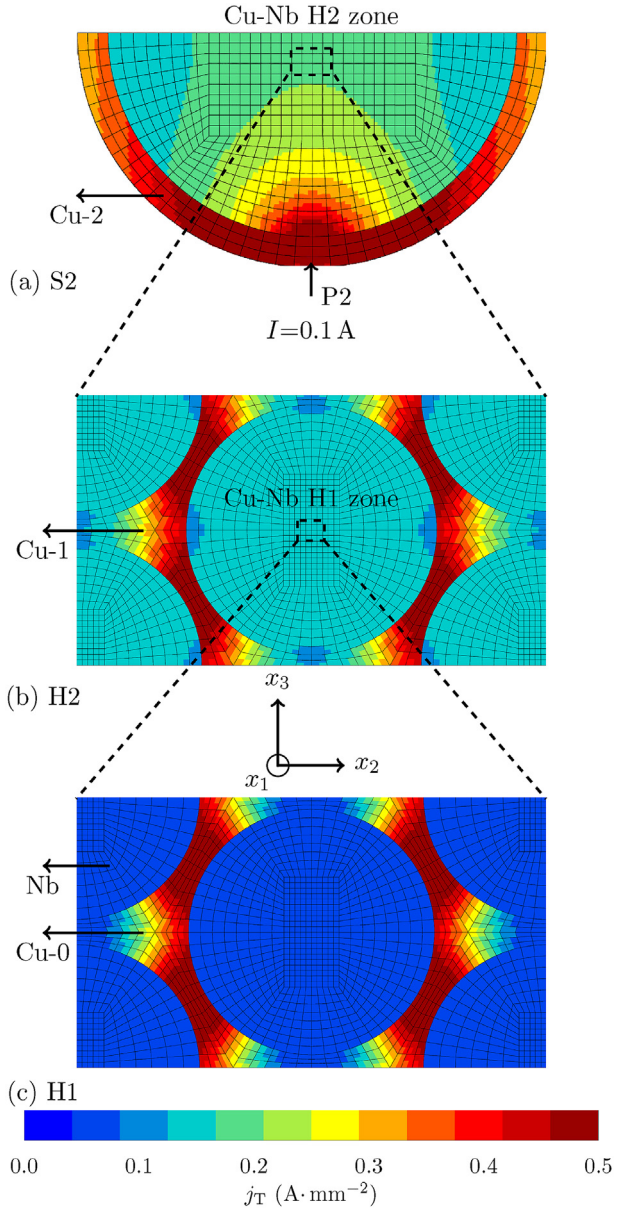

Fig. 8. Transverse current density $j_{\mathrm{T}} = \sqrt{j_2^2 + j_3^2}$ distribution for $N = 85^2$ Cu-Nb Filamentary wires with a diameter of 2.10 mm at (a) scale S2, (b) H2 and (c) H1.

From the experimental comparison of Fig. 7, it follows that the S2/S3 model provides an excellent prediction of the transverse electric conductance for both $N = 85^2$ and 85^3 Cu-Nb Filamentary wires. Furthermore, the transverse conductance depends directly on the homogenized electrical conductivity $(\tilde{\sigma}_{\mathrm{T}})_{\mathrm{H2/H3}}$. In other words, the proposed GSC scheme, PH and scale transition iterative process are validated for the first time by experimental data, especially in the transverse direction for the fiber-reinforced materials.

5.3. Current density distribution in the Cu-Nb composites

The anisotropic effective electrical conductivity $\widetilde{\boldsymbol{\sigma}}$ was predicted by multiscale modeling (Section 4.3) which are validated by experimental data in both longitudinal direction (Section 5.1) and transverse direction (Section 5.2). As shown in Fig. 4, it is found that the effective longitudinal conductivity is always larger than the transverse one $\tilde{\sigma}_{\mathrm{L}} > \tilde{\sigma}_{\mathrm{T}} (\tilde{\sigma}_{\mathrm{L}}/\tilde{\sigma}_{\mathrm{T}} \approx 1.3)$. In this section, our models will provide a quantitative understanding of this anisotropy by exploring the current density distribution at all scales.

The $N = 85^2$ conductor with a diameter of 2.10 mm is chosen here. The transverse current density $j_{\mathrm{T}} = \sqrt{j_2^2 + j_3^2}$ is investigated when sample S2 is numerically subjected to a current $I = 0.1$ A at P2 (mentioned in Section 5.2). Fig. 8(a) indicates the obtained j_{T} distribution at scale S2. A rectangular area corresponding to the H2 RVE size is chosen to determine the average current density $\langle \underline{j} \rangle$. This current density is then injected to the mesh at scale H2. This localization is carried out successively up to H1. The j_{T} distributions at H2 and H1 are shown in Fig. 8(b) and (c) respectively using the same color scale.

It is found that the current density j_{T} displays a non-uniform distribution: about 50% of the Cu channel exhibits a higher j_{T} up to $\sim 0.5\ \mathrm{A}\,mm^{-2}$ than the other part due to the fiber-reinforced microstructure. However, j_{T} in Nb fibers is negligible compared with Cu matrix. Thus, multi-scale modeling demonstrates that current flows along the least resistive path, i.e. within Cu as much as possible, leading to "curved" current lines. On the contrary, when assessed longitudinally, current lines remain parallel to the fibers [22]. In this case, j_{L} (i.e. j_1) exhibit a uniform distribution in each Cu/Nb component. Therefore, experiments and theory find consistently that the Cu-Nb wires exhibit an anisotropic effective conductivity due to the significant influence of their specific microstructure.

6. Conclusions

This work focuses on multiscale modeling of the anisotropic electrical conductivity of architectured and nanostructured Cu-Nb composite wires, then this modeling strategy is validated by experimental data for the first time. The main conclusions of this work are the following:

1. Size effect is considered in models by the definition of the conductivity of each component in the Cu-Nb wires. For instance, bulk polycrystalline Cu exhibits a conductivity of 0.568 $\mu\Omega^{-1}\mathrm{cm}^{-1}$ at 293 K, while the conductivity of long Cu channels with a width as small as 50.9 nm is predicted to be 0.327 $\mu\Omega^{-1}\mathrm{cm}^{-1}$. The size effect taken into account by multiscale modeling of Cu-Nb wires is then confirmed by experiments.
2. Two homogenization models are applied and compared for the determination of the effective electrical conductivity of the

fiber-reinforced microstructure. A mean-field GSC scheme and a full-field FEM PH were proposed assuming a random or periodic distribution of Cu-Nb long fibers respectively. The perfect agreement between the two models reveals a limited influence of fiber distribution on the effective conductivity.

3. An iterative homogenization approach is used to predict the effective electrical conductivity up to scale H2/H3 for $N = 85^2$ and $N = 85^3$ respectively. The effective conductivity estimated by the GSC scheme and PH always almost coincide at all scales.
4. The anisotropic electrical properties of Cu-Nb wires are determined by the four-point probe technique, in particular the transverse conductance is measured for the first time in these materials.
5. The model predictions are successfully compared with experimental data obtained in this work for both longitudinal and transverse conductivities (i.e. $\tilde{\sigma}_L$ and $\tilde{\sigma}_T$). Experiments and theory show consistently that the specific architecture and microstructure of Cu-Nb composites have a significant effect on their anisotropic conductivity (leading to $\tilde{\sigma}_L/\tilde{\sigma}_T \approx 1.3$).

Further work is in progress in the following directions: Cu-Nb wires are used in winding coils for generation of intense magnetic fields (>90 *T*) at 77 K (instead of 293 K studied in this work) [6]. Therefore, theory and experiment will be extended taking various temperatures into account. In addition, the precise values of dislocation density for various conductor diameters and realistic geometrical heterogeneity will be considered in multiscale modeling.

Acknowledgment

The authors gratefully acknowledge the support provided by ANR through the METAFORES ANR-12-BS09-0002 project. This work was supported by Programme Investissements d'Avenir under the program ANR-11-IDEX-0002-02, reference ANR-10-LABX-0037-NEXT.

References

[1] A. Misra, L. Thilly, Structural metals at extremes, MRS Bull. 35 (12) (2010) 965–976.
[2] F. Dupouy, E. Snoeck, M. Casanove, C. Roucau, J. Peyrade, S. Askenazy, Microstructural characterization of high strength and high conductivity nanocomposite wires, Scr. Mater. 34 (7) (1996) 1067–1073.
[3] V. Vidal, Optimisation des propriétés mécaniques des conducteurs nanofilamentaires Cu/X (X=Nb ou Ta) par l'étude des mécanismes élémentaires de déformation, Ph.D. thesis, Docteur de l'Institut National des Sciences Appliquées de Toulouse, Dec. 2006.
[4] S. Lim, A. Rollett, Length scale effects on recrystallization and texture evolution in Cu layers of a roll-bonded Cu–Nb composite, Mater. Sci. Eng. A 520 (1) (2009) 189–196.
[5] I. Beyerlein, J. Mayeur, S. Zheng, N. Mara, J. Wang, A. Misra, Emergence of stable interfaces under extreme plastic deformation, Proc. Natl. Acad. Sci. 111 (12) (2014) 4386–4390.
[6] L. Thilly, Exploration théorique et expérimentale de fils nanocomposites continus présentant des propriétés extrêmes de conductivité électrique et de limite élastique, Ph.D. thesis, Institut national des sciences appliquées de Toulouse, Dec. 2000.
[7] L. Thilly, F. Lecouturier, J. Von Stebut, Size-induced enhanced mechanical properties of nanocomposite copper/niobium wires: nanoindentation study, Acta Mater. 50 (20) (2002) 5049–5065.
[8] K. Spencer, F. Lecouturier, L. Thilly, J. Embury, Established and emerging materials for use as high-field magnet conductors, Adv. Eng. Mater. 6 (5) (2004) 290–297.
[9] J. Béard, J. Billette, P. Frings, M. Suleiman, F. Lecouturier, Special coils development at the national high magnetic field laboratory in Toulouse, J. Low Temp. Phys. 170 (5-6) (2013) 442–446.
[10] B. Halperin, G. Aeppli, Y. Ando, M. Aronson, D. Basov, T. Budinger, R. Dimeo, J. Gore, F. Hunte, C. Lau, et al., High Magnetic Field Science and its Application in the United States: Current Status and Future Directions, National Academy of Sciences: Washington, DC.
[11] L. Frydman, High magnetic field science and its application in the United States: a magnetic resonance perspective, J. Magnetic Reson. 242 (2014) 256–264.
[12] V. Vidal, L. Thilly, F. Lecouturier, P. Renault, Cu nanowhiskers embedded in Nb nanotubes inside a multiscale Cu matrix: the way to reach extreme mechanical properties in high strength conductors, Scr. Mater. 57 (3) (2007) 245–248.
[13] L. Thilly, M. Veron, O. Ludwig, F. Lecouturier, Deformation mechanism in high strength Cu/Nb nanocomposites, Mater. Sci. Eng. A 309 (2001) 510–513.
[14] L. Thilly, S. Van Petegem, P. Renault, F. Lecouturier, V. Vidal, B. Schmitt, H. Van Swygenhoven, A new criterion for elasto-plastic transition in nanomaterials: application to size and composite effects on Cu–Nb nanocomposite wires, Acta Mater. 57 (11) (2009) 3157–3169.
[15] S.-B. Lee, J. LeDonne, S. Lim, I. Beyerlein, A. Rollett, The heterophase interface character distribution of physical vapor-deposited and accumulative roll-bonded Cu–Nb multilayer composites, Acta Mater. 60 (4) (2012) 1747–1761.
[16] B. Hansen, J. Carpenter, S. Sintay, C. Bronkhorst, R. McCabe, J. Mayeur, H. Mourad, I. Beyerlein, N. Mara, S. Chen, et al., Modeling the texture evolution of Cu/Nb layered composites during rolling, Int. J. Plasticity 49 (2013) 71–84.
[17] G. Badinier, C. Sinclair, S. Allain, O. Bouaziz, The Bauschinger effect in drawn and annealed nanocomposite Cu–Nb wires, Mater. Sci. Eng. A 597 (2014) 10–19.
[18] J. Carpenter, R. McCabe, J. Mayeur, N. Mara, I. Beyerlein, Interface-driven plasticity: the presence of an interface affected zone in metallic lamellar composites, Adv. Eng. Mater. 17 (1) (2015) 109–114.
[19] T. Gu, E. Hervé-Luanco, H. Proudhon, L. Thilly, J.-B. Dubois, F. Lecouturier, O. Castelnau, S. Forest, Modélisation multi-échelle du comportement électrique de nano-composites Cu-Nb, Matériaux Tech. 103 (3) (2015) 309.
[20] T. Gu, O. Castelnau, S. Forest, E. Hervé-Luanco, F. Lecouturier, H. Proudhon, L. Thilly, Multiscale modeling of the elastic behavior of architectured and nanostructured Cu-Nb composite wires, Int. J. Solids Struct. 121 (2017) 148–162, http://dx.doi.org/10.1016/j.ijsolstr.2017.05.022.
[21] F. Heringhaus, H.-J. Schneider-Muntau, G. Gottstein, Analytical modeling of the electrical conductivity of metal matrix composites: application to Ag–Cu and Cu–Nb, Mater. Sci. Eng. A 347 (1) (2003) 9–20.
[22] P.K. Mallick, Fiber-reinforced Composites: Materials, Manufacturing, and Design, CRC Press, 2007.
[23] T. Behzad, M. Sain, Measurement and prediction of thermal conductivity for hemp fiber reinforced composites, Polym. Eng. Sci. 47 (7) (2007) 977–983.
[24] K. Schulgasser, Relationship between single-crystal and polycrystal electrical conductivity, J. Appl. Phys. 47 (5) (1976) 1880–1886.
[25] J. Sivardière, Symétrie et propriétés physiques – Du principe de Curie aux brisures de symétrie, EDP Sciences, 2008.
[26] L. Lu, Y. Shen, X. Chen, L. Qian, K. Lu, Ultrahigh strength and high electrical conductivity in copper, Science 304 (5669) (2004) 422–426.
[27] K. Fuchs, The conductivity of thin metallic films according to the electron theory of metals, Math. Proc. Camb. Philosophical Soc. 34 (1) (1938) 100–108, http://dx.doi.org/10.1017/S0305004100019952.
[28] R.B. Dingle, The electrical conductivity of thin wires, Proc. R. Soc. Lond. A: Math. Phys. Eng. Sci. 201 (1067) (1950) 545–560, http://dx.doi.org/10.1098/rspa.1950.0077.
[29] J. Sambles, K. Elsom, T. Preist, The resistivity of thin wires, J. Phys. F: Metal Phys. 12 (6) (1982) 1169.
[30] E.H. Sondheimer, The mean free path of electrons in metals, Adv. Phys. 50 (6) (2001) 499–537.
[31] W. Steinhögl, G. Schindler, G. Steinlesberger, M. Engelhardt, Size-dependent resistivity of metallic wires in the mesoscopic range, Phys. Rev. B 66 (7) (2002) 075414.
[32] W. Steinhögl, G. Schindler, G. Steinlesberger, M. Traving, M. Engelhardt, Comprehensive study of the resistivity of copper wires with lateral dimensions of 100 nm and smaller, J. Appl. Phys. 97 (2) (2005) 023706.
[33] Q. Huang, C.M. Lilley, M. Bode, R. Divan, Surface and size effects on the electrical properties of Cu nanowires, J. Appl. Phys. 104 (2) (2008) 023709.
[34] K. Schulgasser, On the conductivity of fiber reinforced materials, J. Math. Phys. 17 (3) (1976) 382–387.
[35] D. Hasselman, L.F. Johnson, Effective thermal conductivity of composites with interfacial thermal barrier resistance, J. Compos. Mater. 21 (6) (1987) 508–515.
[36] I. Tavman, H. Akinci, Transverse thermal conductivity of fiber reinforced polymer composites, Int. Commun. Heat Mass Transf. 27 (2) (2000) 253–261.
[37] E. Hervé-Luanco, S. Joannès, Multiscale modelling of transport phenomena for materials with n-layered embedded fibres. part I: analytical and numerical-based approaches, Int. J. Solids Struct. 97 (2016) 625–636, http://dx.doi.org/10.1016/j.ijsolstr.2016.05.015.
[38] M.R. Islam, A. Pramila, Thermal conductivity of fiber reinforced composites by the fem, J. Compos. Mater. 33 (18) (1999) 1699–1715.
[39] E. Hervé, A. Zaoui, Elastic behaviour of multiply coated fibre-reinforced composites, Int. J. Eng. Sci. 33 (10) (1995) 1419–1433.
[40] E. Hervé, Thermal and thermoelastic behaviour of multiply coated inclusion-reinforced composites, Int. J. Solids Struct. 39 (4) (2002) 1041–1058.
[41] S. Joannès, E. Hervé-Luanco, Multiscale modelling of transport phenomena for materials with n-layered embedded fibres. part II: investigation of fibre packing effects, Int. J. Solids Struct. 97 (2016) 566–574, http://dx.doi.org/10.1016/j.ijsolstr.2016.06.026.
[42] C. E. NormeInternationale, Méthode de mesure de la résistivité des matériaux métalliques, Tech. rep., Publication CEI 468, 1974.
[43] J. Chan, Four-point Probe Manual, Microfabrication Laboratory, University of

California at Berkeley, Spring.
[44] Y. Kitaoka, T. Tono, S. Yoshimoto, T. Hirahara, S. Hasegawa, T. Ohba, Direct detection of grain boundary scattering in damascene Cu wires by nanoscale four-point probe resistance measurements, Appl. Phys. Lett. 95 (5) (2009) 052110.
[45] F. Smits, Measurement of sheet resistivities with the four-point probe, Bell Syst. Tech. J. 37 (3) (1958) 711–718.
[46] H.-D. Liu, Y.-P. Zhao, G. Ramanath, S. Murarka, G.-C. Wang, Thickness dependent electrical resistivity of ultrathin (< 40 nm) Cu films, Thin Solid Films 384 (1) (2001) 151–156.
[47] J. Dubois, Conducteurs nanocomposites métalliques élaborés par déformation plastique sévère : formation et stabilité thermo-mécanique des nanostructures, propriétés induites, Ph.D. thesis, Université de Poitiers, Dec. 2010.
[48] G. Batchelor, Transport properties of two-phase materials with random structure, Annu. Rev. Fluid Mech. 6 (1) (1974) 227–255.
[49] G.W. Milton, The Theory of Composites, the Theory of Composites, by Graeme W. Milton, Cambridge University Press, Cambridge, UK, May 2002, ISBN 0521781256, p. 748.
[50] J.-R. Medy, Evaluation des effets de taille et d'architecture sur les propriétés mécaniques et électriques de fils composites métalliques cuivre/niobium fabriqués par déformation plastique sévère, Ph.D. thesis, Université de Poitiers, Dec. 2016.
[51] N.W. Ashcroft, N.D. Mermin, Solid State Physics (Saunders College, Philadelphia), 1976. Appendix N.
[52] R. Christensen, K. Lo, Solutions for effective shear properties in three phase sphere and cylinder models, J. Mech. Phys. Solids 27 (4) (1979) 315–330.
[53] T. Kanit, S. Forest, I. Galliet, V. Mounoury, D. Jeulin, Determination of the size of the representative volume element for random composites: statistical and numerical approach, Int. J. solids Struct. 40 (13) (2003) 3647–3679.
[54] J. Besson, G. Cailletaud, J.-L. Chaboche, S. Forest, M. Blétry, Non-linear Mechanics of Materials, vol. 167, Springer, Netherlands, 2010, http://dx.doi.org/10.1007/978-90-481-3356-7.